COMMUNICATION

www.advmat.de

Different Modes of Deformation of Soft Triangular Honeycombs at the Sub-5 nm Scale

Marco Poppe, Changlong Chen, Silvio Poppe, Christoph Kerzig, Feng Liu,* and Carsten Tschierske*

Patterning on the sub-5 nm length scale is a contemporary challenge for further miniaturization of microelectronic circuits. Here, the first soft self-assembled triangular patterns are reported showing transitions between regular and two different kinds of isosceles (acute and obtuse angled) triangles on this length scale, formed by liquid crystalline honeycombs of polyphilic block molecules involving a fluorinated oligo(*para*-phenylene ethynylene) core. The type of formed triangular pattern depends on the degree and position of fluorination and on temperature. They are the first soft honeycombs combining tilted and nontilted organizations in a uniform nanostructure, where the tilted molecules in only one or two sides of the triangular prismatic cells dominate the shape and the size of the morphology.

Nanoscale patterning has advanced in recent years with different kinds of nanostructures. Triangular tiling patterns,[1] for example, were achieved in nets on surfaces,[2–4] with metal–organic[5] and covalent organic frameworks,[6] by means of structural DNA/RNA nanotechnology[7] and with triangular molecules.[8] In soft matter systems honeycombs composed of triangular prismatic cells are known to be formed either by block copolymers[9] on more than 100 nm scale or on a smaller length scale by T-shaped and X-shaped polyphilic block molecules involving a rod-like core-unit.[10] In these honeycombs the shape of the prismatic cells is mainly determined by the ratio between the length of the rigid cores forming the honeycomb walls, and the volume of the lateral chains filling the space inside the resulting prismatic cells.[11] In this case triangular honeycombs were obtained by combination of long rods with comparatively short lateral chains,[10] but all
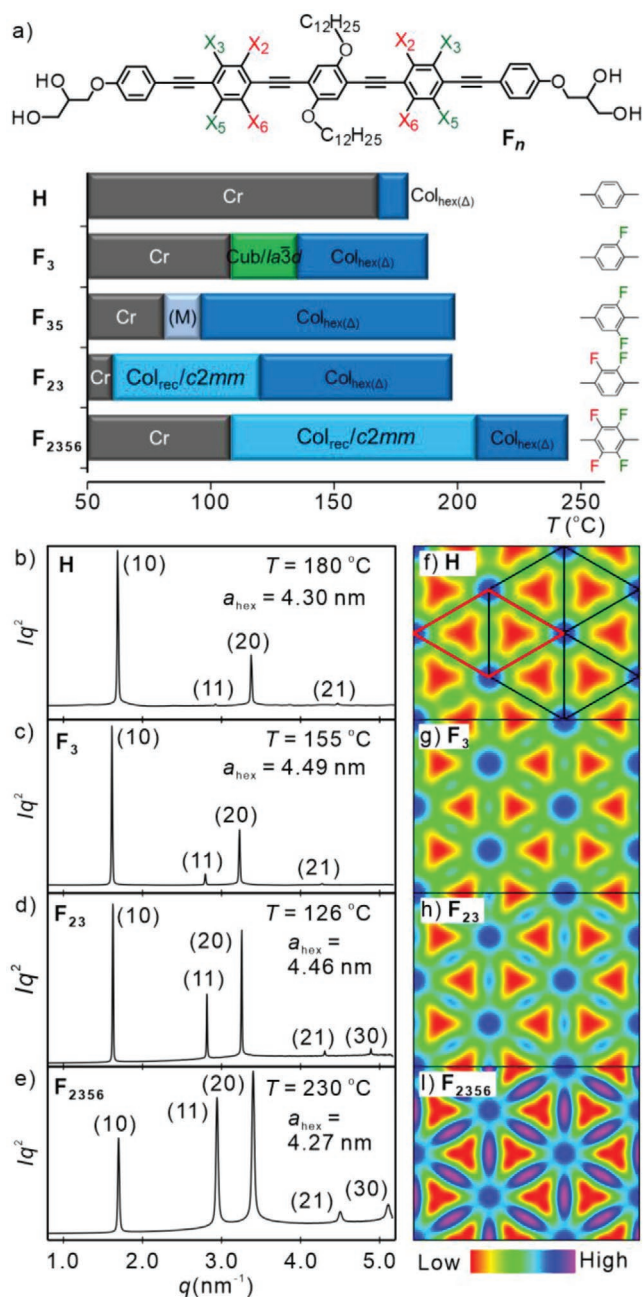
Dr. M. Poppe, Dr. S. Poppe, Dr. C. Kerzig, Prof. C. Tschierske
Department of Chemistry
Martin-Luther-University Halle-Wittenberg
Kurt-Mothes Str. 2, Halle/Saale D-06108, Germany
E-mail: carsten.tschierske@chemie.uni-halle.de
C. Chen, Prof. F. Liu
State Key Laboratory for Mechanical Behaviour of Materials
Shaanxi International Research Center for Soft Matter
Xi'an Jiaotong University
Xi'an 710049, P. R. China
E-mail: feng.liu@xjtu.edu.cn

The ORCID identification number(s) for the author(s) of this article can be found under https://doi.org/10.1002/adma.202005070.

previously reported nanostructures based on a monohedral triangular tiling involved exclusively regular triangles, leading to a hexagonal symmetry of the resulting net or honeycomb. To obtain irregular triangles the input of additional information is required.

Here, we report the first long range periodic soft matter structures composed of isosceles triangles and formed by self-assembly of a single type of molecular rods. The compounds represent X-shaped molecules involving a fluorinated rod-like oligo(*para*-phenylene ethynylene) (OPE) core with sticky hydrogen bonding glycerol units at both ends and two soft dodecyloxy side-chains at opposite sides of the OPE cores, inhibiting their clustering into layers. For the parent nonfluorinated compound **H** (see **Figure 1**) with two dodecyloxy chains and all X = H, the formation of a hexagonal columnar liquid crystalline (LC) phase based on a regular triangular honeycombs was observed (Col$_{hex(\Delta)}$ phase).[12] Fluorination of the peripheral benzene rings removes the triangular honeycomb and replaces it by a bicontinuous cubic phase (Cub$_{bi}$, see Figure S10, Supporting Information).[13] The effect of fluorination of the two inner benzene ring adjacent to the donor-substituted central ring, leading to an alternating donor–acceptor system is reported herein. It was found that for these compounds the triangular honeycomb structure is retained and stabilized. Even more interestingly, at lower temperature the triangular prismatic cells become distorted by tilting of the OPEs in some of the honeycomb walls, thus leading to new rectangular columnar LC phases composed of isosceles triangular prismatic cells.

The synthesis of the X-shaped compounds F_n, was carried out in a sequence of Sonogashira cross coupling reactions[14] as outlined in the Supporting Information. An overview over the phase sequences of the fluorinated compounds F_n compared to the non-fluorinated compound **H**[12] is shown in Figure 1a (for numerical data, see Table S1 in the Supporting Information). In general, fluorination of the two inner benzene rings widens the LC phase range by reduction of the melting point and stabilizes the LC phases.[15] The most dramatic stabilizing effect by +64 K compared to compound **H** is found for F_{2356} involving two tetrafluorinated rings. The effect of the electrostatic π–π interactions between aromatic units[16a,b] is obviously stronger than the steric distortion due to the bulkier fluorines and thus stabilizes LC self-assembly.[16c,d]

All compounds F_n show a hexagonal columnar mesophase with *p6mm* symmetry on cooling from the isotropic liquid, as indicated by the typical textures (Figures S2a,c,e and S3a, Supporting Information) and, the sharp Bragg reflections in small-angle X-ray scattering (SAXS) showing the reciprocal *d*-spacings in the ratio

Figure 1. a) Structure (subscript n indicates the position(s) of the F-atom(s)) and LC phases of compounds F_n (recorded by DSC on cooling, 10 K min^{-1}) in comparison with compound H (all X = H);[12] for numerical data, transitions on heating, DSC traces and transition enthalpies, see Table S1 and Figure S1 (Supporting Information); abbreviations: Cr = crystalline solid, $Col_{hex(\Delta)}$ = hexagonal columnar LC phase with triangular honeycomb structure and $p6mm$ plane group; $Cub/Ia\bar{3}d$ = Cub_{bi} phase with $Ia\bar{3}d$ space group (double gyroid, see Figure S10, Supporting Information), M = unknown mesophase, $Col_{rec}/c2mm$ = rectangular columnar LC phases with isosceles triangular honeycomb structure and $c2mm$ plane groups (see Figure 2); b–e) SAXS diffractograms of the $Col_{hex(\Delta)}/p6mm$ phases of compounds H and F_n; f–i) reconstructed ED maps (for details, see Supporting Information). The red lines in (f) indicate a unit cell and black lines indicate the triangular tiling pattern of the OPE cores.

1: $3^{1/2}$: 2... etc. (Figure 1b–e). The diffuse wide-angle X-ray scattering (WAXS) with a maximum at $d = 0.42$–0.46 nm evidences the absence of positional long range order between the individual molecules, thus confirming LC phases (**Figure 2**d,h; Figure S7, Supporting Information). For compounds with two or four fluorines at each inner ring, (F_{35}, F_{23}, and F_{2356}) there exists a clear shoulder at $d \approx 0.36$ nm, indicating a strong π–π interaction between the OPE cores; the intensity grows with increasing degree of fluorination and decreasing temperature (Figure 2d,h; Figure S7b, Supporting Information). The formation of these Col_{hex} phases with a triangular honeycomb structure ($Col_{hex(\Delta)}$)[10] is corroborated by the reconstructed electron density (ED) maps shown in Figure 1f–i. The high ED dots (blue/purple) on the hexagonal lattice represent the projection of the columns formed by the hydrogen-bonded glycerol units. These are connected by the OPE cores which have growing ED with increasing number of fluorines (from green for F_3 via blue for F_{23} to purple for F_{2356}) and the triangular cells are filled by the low ED (yellow/red) flexible alkyl chains. Since the hexagonal lattice parameter ($a_{hex} = 4.27$–4.49 nm) is almost the same as the molecular length ($L_{mol} = 4.2 \pm 0.2$ nm)[17] (Table S9, Supporting Information), an organization of the molecular rods in a triangular honeycomb takes place without molecular tilting.

Compound F_3, having only one fluorine at each inner edge-position, has a cubic phase at lower temperature, characterized by the optical isotropic appearance, i.e., by being completely dark between crossed polarizers (Figure S2b, Supporting Information), as well as by its viscoelasticity and the typical XRD pattern, indexed to be a cubic $Ia\bar{3}d$ lattice ($a_{cub} = 9.29$ nm, Figure S5 and Table S3, Supporting Information). In this Cub_{bi} phase the aromatic cores are arranged on the gyroid minimal surface and the polar glycerols form two infinite networks (Figure S10, Supporting Information).[13] Introduction of a second fluorine in each of the inner benzene rings widens the $Col_{hex(\Delta)}$ range, stabilizes the $Col_{hex(\Delta)}$ phase and removes the cubic phase (Figure 1) which is replaced by columnar phases with reduced symmetry. Compound F_{35}, having exclusively edge-directed fluorines, forms an unknown phase whose structure is not yet solved (M-phase). Compounds F_{23} and F_{2356} combining edge and core directed fluorine substituents at the inner benzene rings form the triangular honeycomb as high temperature phase too, and show a phase transition to columnar phases with rectangular lattice (see Figure 2).

The SAXS pattern of the low temperature phase of compound F_{23} (Figure 2a) is indexed to be a centered rectangular $c2mm$ lattice with lattice parameter $a_{rec} = 7.70$ nm and $b_{rec} = 3.74$ nm ($Col_{rec(\Delta)}/c2mm$) at 106 °C. The reconstructed ED map (Figure 2b) evidences a triangular honeycomb, squashed along the direction b. The purple/blue high ED dots show the positions of the projection of the columns formed by the glycerols and the central fluorinated parts of the aromatic cores (light blue) connect the columns. As in the case of the $Col_{hex(\Delta)}$ phases the spaces enclosed by the triangular cells have low ED (yellow/red) and are filled by the alkyl chains. The parameter $a_{rec} = 7.70$ nm remains approximately the same as the distance along direction a in the hexagonal lattice ($d_a = 3^{1/2} a_{hex} = 7.72$ nm) whereas $b_{rec} = 3.74$ nm is considerably reduced ($d_b < a_{hex} = 4.43$ nm, see also Figure 2c and Table S5, Supporting Information). This could be interpreted as a transition from regular to isosceles triangular honeycombs by a tilt of the molecules aligned
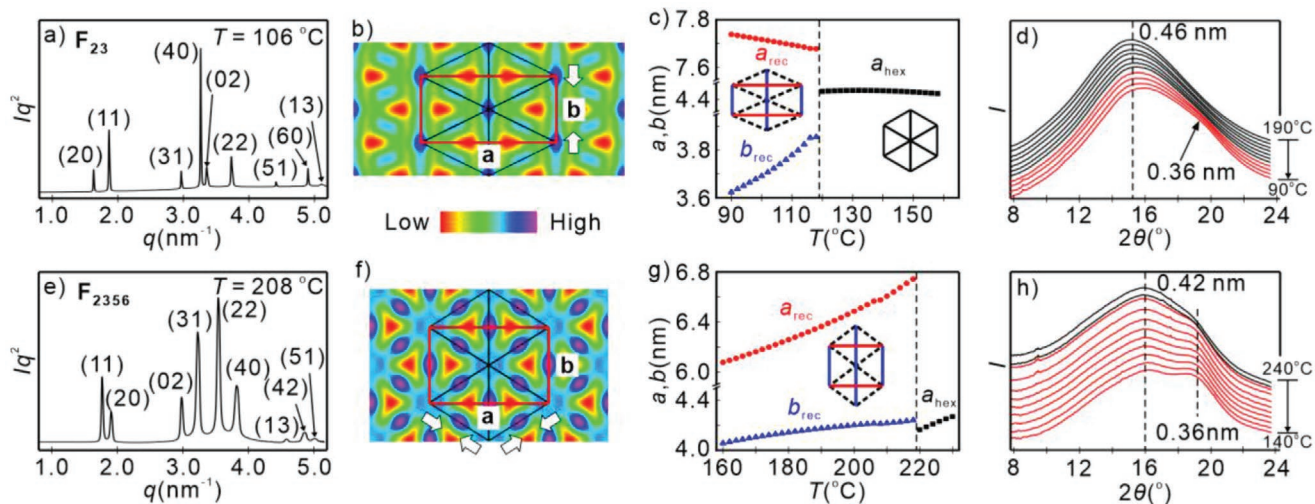
Figure 2. a–h) $Col_{rec(\Delta)}/c2mm$ phases of compounds F_{23} (a–d) F_{2356} (e–h): a,e) SAXS diffractograms; b,f) reconstructed ED maps (for details, see Supporting Information); c,g) development of lattice parameters upon cooling; d,h) WAXS diffractograms upon cooling (black curves for $Col_{hex(\Delta)}$ and red for $Col_{rec(\Delta)}$). For phase transition temperatures and enthalpies, see Table S1 and Figure S1c,d in the Supporting Information.
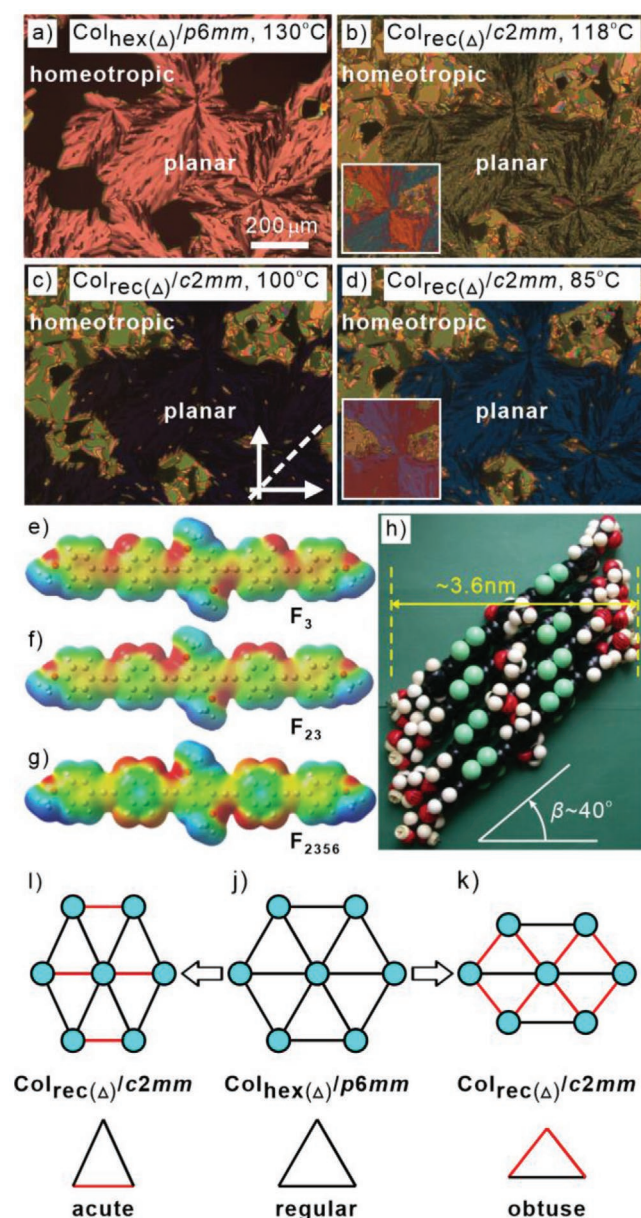
along direction b (those shown in blue in Figure 2c), whereas those in all others walls (shown in dash black lines) remain non-tilted. The tilt angle with respect to the normal of the prismatic cells is estimated according to $cos\beta = b_{rec}/L_{mol}$ ($L_{mol} = 4.5$ nm $= a_{hex}$) to be around $\beta = 33.4°$ at 106 °C, and shifted toward a maximum of around 36.4° during the continuous cooling. This angle is close to the magic angle of 36.3° which is reached at $T = 100$ °C (see explanations in Figure S4 in the Supporting Information). At this temperature the planar sample becomes optically isotropic (**Figure 3**b→c) and the sign of birefringence changes from being negative as typical for the polygonal honeycombs to weakly positive (Figure 3d and insets in Figure 3b,d). It is proposed that in these areas with spherulitic-like texture the dominating orientation of the columns is parallel to the substrate surfaces with the sides formed by the tilted molecules arranged parallel to the surface. This orientation is preferred due to the easier bending of the cylinders of the $Col_{rec(\Delta)}$ phase with tilted organization of the molecules. In this case the tilted molecules have the major influence on the birefringence, but the two other faces contribute with their projection and therefore the critical angle for $\Delta n = 0$ corresponds to the magic angle (for details, see Figure S4 in the Supporting Information).

In the dark homeotropic areas of the uniaxial $Col_{hex(\Delta)}$ phase (Figure 3a) the columns are arranged perpendicular to the surfaces and therefore it always appears optically isotropic if viewed along the columns. Depending on the surfaces and the alignment conditions either of these alignments, planar or homeotropic, can be obtained selectively. In an (almost) uniformly homeotropic alignment of the $Col_{hex(\Delta)}$ phase with a surface tiling by regular triangles (Figure S3h, Supporting Information) a birefringent mosaic texture develops at the transition to the biaxial $Col_{rec(\Delta)}/c2mm$ phase (Figure 3a→b) with uniform orientation of the 2D lattice, i.e., uniform direction of the acute angled triangles over areas covering several 100 μm^2 (Figure S3h→i, Supporting Information). This transition is reversible and an isotropic texture is recovered at the transition back to the uniaxial hexagonal lattice with nondeformed triangles on heating (Figure S3i→j, Supporting Information).

Compound F_{2356} having four instead of only two fluorines at each inner ring shows a similar phase sequence on cooling as compound F_{23} (Figure 1a). However, the ratio of a_{rec}/b_{rec} is very distinct from that found for the $c2mm$ phase of F_{23}. Taking the diffraction pattern at 208 °C as an example (Figure 2e), the lattice parameter $b_{rec} = 4.21$ nm is almost equal to a_{hex}, in contrast, $a_{rec} = 6.58$ nm is much smaller than the calculated distance $d = 3^{1/2}a_{hex} = 7.40$ nm in the hexagonal lattice. This means that in this case the rods forming the honeycomb walls in direction b are nontilted or only weakly tilted, whereas those in the remaining walls are significantly tilted (see Figure 2f,g), thus being just the other way around than observed for F_{23}. The tilt is estimated according to $cos\beta = [(a_{rec}/2)^2 + (b_{rec}/2)^2]^{1/2}/L_{mol} = 3.91/4.5$ as $\beta = 29.8°$, and developed a maximum of 35.7° upon continuous cooling. That the fundamental structure once again represents an isosceles triangular tiling is evident from the reconstructed ED map, shown in Figure 2f. Though in this structure the ratio between tilted and nontilted walls is 2:1, the planar textures (columns parallel to the substrate surfaces) has relatively high birefringence which becomes smaller at the $Col_{hex(\Delta)}–Col_{rec(\Delta)}$ phase transition (Figure S2e,f, Supporting Information), though it never goes through zero.[18] Similarly, the WAXS results show a stronger shoulder at $d = 0.36$ nm in addition to the one at $d = 0.42$ nm (Figure 2h), indicating a stronger face-to-face $\pi–\pi$ stacking in F_{2356}. This is in line with the higher degree of fluorination of the two inner benzene rings. The increased donor-acceptor interactions obviously make it more difficult to avoid the longitudinal shift of the rods and hence support the tilt of the aromatic cores. Also, for this compound homeotropic alignment can be achieved, showing similar textural changes at the phase transition (Figure S2g–h, Supporting Information), as those discussed for F_{23}.

Overall, the number of tilted honeycomb walls per unit cell increases with growing fluorination from F_{23} with only one tilted to F_{2356} involving two tilted walls around each triangular prismatic cell. If the electrostatic surface potentials maps of the OPE cores of compounds F_3, F_{23}, and F_{2356} are compared (Figure 3e–g), the electron density of the π-faces of the inner

**ADVANCED
SCIENCE NEWS**

www.advancedsciencenews.com

**ADVANCED
MATERIALS**

www.advmat.de

Figure 3. a–d) Transition from $Col_{hex(\Delta)}/p6mm$ to $Col_{rec(\Delta)}/c2mm$ of compound F_{23} as observed by polarizing microscopy in the indicated phases at the given temperatures; the insets in (b,d) show the textures with additional λ-retarder plate, indicating negative birefringence in (b) and positive birefringence in (d); the direction of the polarizers is shown by arrows and the indicatrix slow axis by a dashed line in (c); for more details, see Figures S3 and S4 in the Supporting Information. e–g) Comparison of the electrostatic surface potential maps of model compounds for F_3, F_{23}, and F_{2356} (with $n = 1$) as determined by DFT calculation (B3LYP functional and 6–31G basis set, for F_{35}, see Figure S12 in the Supporting Information); red indicates high and blue low negative surface potential; h) shows the staggered arrangement of F_{2356} in the tilted cylinder walls of the $Col_{rec(\Delta)}/c2mm$ phase with π-stacking between the tetrafluorobenzene acceptor units and the adjacent triple bonds as donors, leading to a tilt of $\approx 40°$; i–k) models showing the organization of the rods in the distinct triangular honeycombs, red lines represent the deformation directions of the triangles; for 3d models and possible modes of tilt correlation, see Figure S11 in the Supporting Information.

benzene rings decreases with increasing fluorination (color changes from yellow to green) whereas the surface potential of the outer rings and especially the acetylene units remains relatively high. Thus, a main contribution to mesophase stabilization and development of tilt is assumed to result from an increasing contribution of electrostatic interactions between the electron deficit fluorinated benzenes with the electron rich acetylene units of the adjacent molecules.[15] This requires a longitudinal shift of the aromatics which leads to a tilt in the range of $\approx 40°$ (Figure 3h), being close to the experimentally observed tilt β. The increasing contribution of π–π stacking is also in line with the WAXS patterns (Figure 2h). Whereas the shoulder at $d \approx 0.36$ nm develops gradually stronger from F_3, F_{23} to F_{2356}, this scattering is still diffuse in all cases, which indicates a short correlation length of π–π stacking, and that the system is still in the fluid state. In addition to the molecular mobility the rotational barrier around the C–C bonds along the OPE core is less than 10 kJ mol^{-1},[19] leading to a fast equilibrium of different rotamers.[20]

To explain the origin of the formation of prismatic cells enclosed by shells composed of sides involving tilted and others involving nontilted rods, it must be considered that the space required by the alkyl chains decreases with lowering temperature and the space inside the triangular cells can be adjusted by tilting. Because efficient π–π stacking requires a certain fixed tilt angle close to 40°, tilting is not possible for all three walls as this would reduce the available space too much to accommodate the lateral chains. In the case of F_{23} with weak π–π stacking, the ratio of tilted and nontilted molecules is 1:2.[21] While in the case of F_{2356} the strongest driving force for tilted organization requires that most molecules become tilted, two thirds of them tilt significantly while only one third does not tilt or tilts only slightly. Thus, there is a delicate balance of competitive π–π stacking and temperature dependent space filling effects, which determines the mode of deformation of the triangular cells (Figure 3i–k).

In summary, aromatic fluorination of X-shaped bolapolyphilic OPEs at the inner benzene rings stabilizes triangular honeycombs (Figures 1a and 3j). The packing of the cores along the cylinder walls becomes denser due to polar interactions between the electron deficit fluorinated rings and the electron rich acetylenes, the developing π-stacking requires a longitudinal shift which then leads to a significant tilt of the molecules in the cylinder walls, thus providing two new types of triangular honeycombs composed of isosceles triangular prismatic cells, being either acute or obtuse angled (Figure 3i,k). These tunable soft triangular patterns have potential for use in nanoscale patterning and for soft nanolithography with regular and nonregular triangular patterns on the sub-5 nm length scale. Furthermore, the combination of different modes of π-stacking in these uniform LC soft matter structures could lead to promising materials for photophysical and charge carrier applications.[22]

Supporting Information

[1] J. A. Millan, D. Ortiz, G. van Anders, S. C. Glotzer, *ACS Nano* **2014**, *8*, 2918.

[2] a) B. Cirera, L. Đorđević, R. Otero, J. M. Gallego, D. Bonifazi, R. Miranda, D. Ecija, *Chem. Commun.* **2016**, *52*, 11227; b) A. Klaiber, S. Polarz, *ACS Nano* **2016**, *10*, 10041; c) D. Écija, J. I. Urgel, A. C. Papageorgiou, S. Joshi, W. Auwärter, A. P. Seitsonen, S. Klyatskaya, M. Ruben, S. Fischer, S. Vijayaraghavan, J. Reichert, J. V. Barth, *Proc. Natl. Acad. Sci. USA* **2013**, *110*, 6678.

[3] I. Hisaki, S. Nakagawa, N. Tohnai, M. Miyata, *Angew. Chem., Int. Ed.* **2015**, *54*, 3008.

[4] a) V. Stepanenko, R. Kandanelli, S. Uemura, F. Würthner, G. Fernández, *Chem. Sci.* **2015**, *6*, 5853; b) R. Zhang, L.-C. Wang, M. Li, X.-M. Zhang, Y.-B. Li, Y.-T. Shen, Q.-Y. Zheng, Q.-D. Zeng, C. Wang, *Nanoscale* **2011**, *3*, 3755; c) W. Xiao, X. Feng, P. Ruffieux, O. Gröning, K. Müllen, R. Fasel, *J. Am. Chem. Soc.* **2008**, *130*, 8910; d) D. Würsch, R. May, G. Wiederer, S. S. Jester, S. Höger, J. Vogelsang, J. M. Lupton, *Chem. Commun.* **2017**, *53*, 352.

[5] a) H. Furukawa, K. E. Cordova, M. O'Keeffe, O. M. Yaghi, *Science* **2013**, *341*, 1230444; b) Z. R. Herm, B. M. Wiers, J. A. Mason, J. M. v. Baten, M. R. Hudson, P. Zajdel, C. M. Brown, N. Masciocchi, R. Krishna, J. R. Long, *Science* **2013**, *340*, 960; c) P. J. Waller, F. Gándara, O. M. Yaghi, *Acc. Chem. Res.* **2015**, *48*, 3053.

[6] a) Y. He, Y. Tian, A. E. Ribbe, C. Mao, *J. Am. Chem. Soc.* **2006**, *128*, 15978; b) I. Hisaki, S. Nakagawa, N. Ikenaka, Y. Imamura, M. Katouda, M. Tashiro, H. Tsuchida, T. Ogoshi, H. Sato, N. Tohnai, M. Miyata, *J. Am. Chem. Soc.* **2016**, *138*, 6617.

[7] a) F. Zhang, Y. Liu, H. Yan, *J. Am. Chem. Soc.* **2013**, *135*, 7458; b) W. W. Grabow, L. Jaeger, *Acc. Chem. Res.* **2014**, *47*, 1871.

[8] Y. Beldjoudi, A. Narayanan, I. Roy, T. J. Pearson, M. M. Cetin, M. T. Nguyen, M. D. Krzyaniak, F. M. Alsubaie, M. R. Wasielewski, S. I. Stupp, J. F. Stoddart, *J. Am. Chem. Soc.* **2019**, *141*, 17783.

[9] a) S. Sioula, N. Hadjichristidis, E. L. Thomas, *Macromolecules* **1998**, *31*, 8429; b) Y. Matsushita, *Macromolecules* **2007**, *40*, 771.

[10] a) F. Liu, B. Chen, U. Baumeister, X. Zeng, G. Ungar, C. Tschierske, *J. Am. Chem. Soc.* **2007**, *129*, 9578; b) X. Cheng, X. Dong, G. Wei, M. Prehm, C. Tschierske, *Angew. Chem., Int. Ed.* **2009**, *48*, 8014; c) W. Bu, H. Gao, X. Tan, X. Dong, X. Cheng, M. Prehm, C. Tschierske, *Chem. Commun.* **2013**, *49*, 1756; d) X. Cheng, H. Gao, X. Tan, X. Yang, M. Prehm, H. Ebert, C. Tschierske, *Chem. Sci.* **2013**, *4*, 3317; e) S. Poppe, M. Poppe, H. Ebert, M. Prehm, C. Chen, F. Liu, S. Werner, K. Bacia, C. Tschierske, *Polymers* **2017**, *9*, 471.

[11] a) C. Tschierske, *Chem. Soc. Rev.* **2007**, *36*, 1930; b) C. Tschierske, C. Nürnberger, H. Ebert, B. Glettner, M. Prehm, F. Liu, X.-B. Zeng, G. Ungar, *Interface Focus* **2012**, *2*, 669; c) C. Tschierske, *Angew. Chem., Int. Ed.* **2013**, *52*, 8828; d) S. Poppe, A. Lehmann, A. Scholte, M. Prehm, X. Zeng, G. Ungar, C. Tschierske, *Nat. Commun.* **2015**, *6*, 8637.

[12] S. Werner, H. Ebert, B.-D. Lechner, F. Lange, A. Achilles, R. Bärenwald, S. Poppe, A. Blume, K. Saalwächter, C. Tschierske, K. Bacia, *Chem. - Eur. J.* **2015**, *21*, 8840.

[13] M. Poppe, C. Chen, F. Liu, S. Poppe, C. Tschierske, *Chem. - Eur. J.* **2017**, *23*, 7196.

[14] K. Sonogashira, Y. Tohda, N. Hagihara, *Tetrahedron Lett.* **1975**, *16*, 4467.

[15] Though the increased average electrostatic core-core interactions stablize the dynamic LC phases, the effect of fluorination on the stability of the crystalline phases is more complex, because it is determind by specific local interactions and details of the molecular packing possibilities in the solid state.

[16] a) C. R. Martinez, B. L. Iverson, *Chem. Sci.* **2012**, *3*, 2191; b) K. Kishikawa, *Isr. J. Chem.* **2012**, *52*, 800; c) Y. Xu, Y. Hu, Q. Chen, J. Wen, *J. Mater. Chem.* **1995**, *5*, 219; d) M. Hird, *Chem. Soc. Rev.* **2007**, *36*, 2070.

[17] M. Poppe, C. Chen, S. Poppe, F. Liu, C. Tschierske, *Commun. Chem.* **2020**, *3*, 70.

[18] As in this case no clear conlusions concerning the alignment of the cylinder faces with respect to the surfaces can be drawn, the precise critical angle cannot be determined with certainty, it is likely to be 45°, especially if anticlinic tilt correlation would be dominating.

[19] M. Kondo, D. Nozaki, M. Tachibana, T. Yumura, K. Yoshizawa, *Chem. Phys.* **2005**, *312*, 289.

[20] For F_{23}, the energy difference between the rotamers with synplanar and antiplanar orientation of the C−F bonds was calculated as 4 kJ mol^{-1} by DFT methods, see Figure S14, allowing a fast equilibrium with a slight preference for the "anti-rotamer". However, due to this dynamic the specific effect of C-F orientation on the LC self assembly is expected to be small.

[21] Note that as the lattice parameter b shrinks, a_{rec} expands a little to keep the volume decreasing not too much with lowering temperature (Figures 2c and S6).

[22] Already in solution compounds **H** and F_{2356} have promising photochemical properties such as pronounced visible-light absorption, blue-light emission and an attractive HOMO–LUMO gap, see Figures S13 and S15.